EVALUATING EFFECTS OF IMAGING PARAMETERS ON SINGLE CELL DETECTION IN MOLECULAR MRI VIA SIMULATION

Ali-Reza Mohammadi-Nejad[1], G.-Ali Hossein-Zadeh[1], and Hamid Soltanian-Zadeh[1,2]
[1]Control and Intelligent Processing Center of Excellence, ECE Dept, Univ. of Tehran, Tehran, Iran,
[2]Medical Image Analysis Lab., Henry Ford Health System, Detroit, Michigan, USA
a.mohammadinejad@ece.ut.ac.ir, ghzadeh@ut.ac.ir, hamids@rad.hfh.edu

ABSTRACT

To evaluate the sensitivity and specificity of MR acquisition methods for molecular imaging, we extended a magnetic resonance imaging (MRI) simulator. This simulator is capable of complete modeling of object (tissue) in microscopic level to study the effect of spatial distribution and concentration of nanoparticles. Using this tool we studied Gradient-Echo (GE), and True-FISP pulse sequences. In terms of detection sensitivity, GE and True-FISP detected individual labeled cells in 9.4 T MRI. We then conducted a systematic study in order to determine the optimal parameters for GE and True-FISP pulse sequences (echo time, repetition time, iron mass per cell, and image resolution). This simulation study provides a basis for planning experiments aimed at single cell detection with GE and True-FISP sequences.

Index Terms— *single cell detection, magnetic resonance imaging (MRI) simulation, superparamagnetic iron-oxide particles (SPIO), pulse sequence, optimal parameters*

1. INTRODUCTION

The most common strategy for visualizing cellular populations or molecular targets in magnetic resonance imaging (MRI) is to label them with superparamagnetic iron-oxide particles (SPIOs). The dipole field originating from the SPIOs locally changes the intensity of T_2^*-weighted images.

Magnetically labeled cells have been used to study a variety of cellular events in medical research including stem cell and immune cell [1] migration, brain ischemia, macrophage infiltration [2], T-cell trafficking, and cancer [3]. In particular, SPIOs have been used to label and track a variety of cell types, with minimal impact on cell function over a period of several weeks. However, monitoring of stem cell homing or T-cell trafficking may involve very small numbers of cells. For example, only a tiny fraction of injected stem cells reach their target sites. Non-invasive imaging methods capable of detecting individual cells would therefore be extremely useful.

The intensity of MRI signal originating from each tissue is mainly determined by three parameters: the local proton density and the two magnetic relaxation times, T_1 and T_2. However, locally different fields or inhomogeneous media, i.e., media with different magnetic susceptibilities, can also be the source of a T_2 shortening. These effects are usually called T_2^* or susceptibility effects. In previous work, detection of SPIO-labeled cells has been accomplished through T_1 [3], T_2 [4], and T_2^*-weighted [5] acquisitions. But, T_2- and T_1-weighted acquisitions can be two or three orders of magnitude less sensitive to SPIO labeled cells, respectively, than T_2^* measurements [6].

Increasing the sensitivity of MRI protocols to SPIO-labeled cells has been a challenge in recent years. By refining the MR hardware (magnetic field intensity, receiver coils, imaging pulse sequences), and cell labeling modalities, some authors have detected single cells, not only *in vitro* [7,8] but also *in vivo* [9]. Detection sensitivity of SPIO labeled cells depend on a number of factors, including static magnetic field strength, SNR, pulse sequence and acquisition parameters such as resolution, echo time (TE), and repetition time (TR), as well as details of the SPIO loading and compartmentalization [8].

In [5], a technique was developed to detect SPIO loaded cells using True-FISP (fast imaging with steady precession) imaging. This sequence (also known as FIESTA (fast imaging employing steady-state acquisition) or b-SSFP (balanced steady-state free precession) is investigated since it has previously been shown to provide exceptional sensitivity to SPIO loaded cells [7], high SNR efficiency, and a Spin-Echo (SE) like insensitivity to background magnetic field inhomogeneity. Reference [10] investigated the detection of single cells in a 9.4 T MRI device. The authors showed that high resolution GE pulse sequences detected individual labeled cells, whereas SE sequences were poorly sensitive to local cell magnetization. Then, they reveal that, the signal loss produced by labeled cells enhanced and spread spatially with increasing TE on GE sequences, and diminished rapidly with increasing voxel size. In [11] the authors have investigated, with computer simulations and experiments at 17.6 T, how the CRAZED experiment can be used to visualize such SPIOs in labeled cells. A critical feature of all above experimental studies is the cost of organizing imaging

sessions with an MRI scanner. However, as a supplement to experiments (which is performed in an MRI scanner), numerical simulations of MRI pulse sequences provide additional insight into the process of image formation, and it can be done via personal computers. Whereas optimization of MRI pulse sequences and parameters is experimentally expensive, it can be easily accomplished through a simulator without significant cost. The simulators are mostly based on the numerical solutions of the Bloch equations.

In Section 2, we will propose a method for simulating the effects of single labeled cell and MRI techniques on imaging such cells. Section 3 introduces the results of simulating various pulse sequences including, the influence of TE, TR, resolution, and iron mass per cell. Conclusions are presented in the final section.

2. METHODS

The effect of each labeled cell on the surrounding magnetic field is usually modeled with a dipole pattern in which the local B_z field is enhanced in the north and south poles and suppressed along the equator [12]. In practice, agglomerations of labeled cells may not be spherical, but they can be assumed to from a group of spheres. The field perturbation caused by a spherical object (in the spherical coordinate) can be written as:

$$\Delta B_z(r,\theta,\varphi) = \frac{\Delta\chi B_0}{3}\left(\frac{a}{r}\right)^3\left(3\cos^2\theta - 1\right) \qquad (1)$$

where $\Delta\chi$ is the difference in bulk magnetic susceptibility between the sphere and surroundings, a is the radius, r is the distance from the sphere center, and θ is the angle relative to the main field, B_0 [12].

The radius of each iron-oxide core is about 4.6 nm. This is derived using the known density of iron-oxide (3.76 gFe/cm^3) [13]. On the other hand, for a given mass of these particles, according to [14], they can not aggregate to each other, and there is a distance between them. In this paper, the distance between particles is considered 1.5 times of their radius. In our simulations, we used different iron masses per labeled cell including 2.5, 4, 4.8, 5.6, and 6.2 picograms. For each concentration, we derived the radius of labeled cell with the above rule of thumb.

We use 3-dimensional (3D) pulse sequences. Also, we simulate intra-voxel field inhomogeneity to be able to evaluate effects of the labeled cells. The spatial resolution of the virtual object (model of tissue) is in a microscopic level. On the other hand, the spatial resolution of image can be determined by pulse sequence and it is usually coarser than that of the model. By this technique, 8×8×8 voxels of virtual object are mapped to one pixel of the resulting image. The static magnetic field (B_0) used in these simulations is equal to 9.4 T. We simulate a 0.64×0.64×0.64 mm^3 object of water with 40×40×40 μm^3 voxel-size containing a single cell in its center. The radius of this cell is equal to 20 μm. Thus, this cell can be completely placed in a voxel. For the sake of reducing the computational complexity in 3D imaging, the virtual object's matrix size is set to 128×128×128, and matrix size of the output image is 16×16×16. Furthermore, all iron oxide particles are placed in the center of the cell and voxel. For the best comparison between our simulation and experimental results in [10], we use a gradient with 2 T/m amplitude in each pulse sequence. The simulated pulse sequences and their parameters are as the following: GE pulse sequence with TR=200 ms, flip angle equal to the Ernest angle; True-FISP pulse sequence with TE=30 ms, flip angle equal to the optimal angle.

We used the open source SIMRI simulator [15] which was implemented using Microsoft Visual C++ 6.0. SIMRI includes an efficient T_2^* management for simulating spin echoes properly. Of course, in order to do a realistic simulation of molecular MRI, we made some changes in this simulator. This includes the capability of virtual object simulation in microscopic level (independent of output-image pixel-size).

As previously mentioned, our main goal in this paper is to show the effect of the parameters of GE and True-FISP pulse sequences on the detection of nanoparticles. These parameters include: TE, TR, and image resolution. We also study the effect of iron mass which is added to the cell for its labeling and detection via MR imaging. Furthermore, we use the Weber ratio [16] as a measure of contrast to quantify the resulting images. Our virtual phantom is made of water (T1=500 ms, T2=77 ms [5]) that includes a labeled cell in its center. This labeled cell decreases the intensity of the output image. According to the Weber-ratio, the minimum change (decrease) required for human eye to detect the cell in the output image is 8 gray levels (if intensity of the background is 253).

3. RESULTS

Figure 1 shows the output images of simulated True-FISP and GE pulse sequences. Consistent with previous experimental work [5], True-FISP is more sensitive than GE for detection of a single labeled cell. Also, the labeled cell affects both upper and lower image slices. The nanoparticles is placed in the center of the labeled cell, therefore, it has relatively symmetric effects in the upper and lower slices.

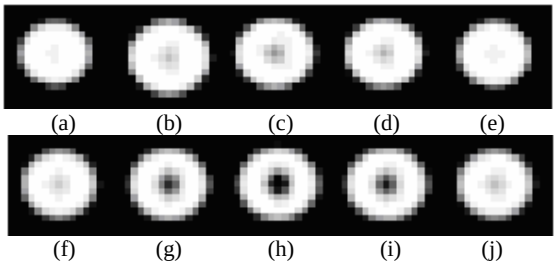

Fig. 1. Detection of single cell with high-resolution MRI (iron mass per cell=5.6 pg) (a, b, c, d, e) 7th, 8th, 9th, 10th, and 11th slices containing a labeled cell with GE pulse sequence (*TE*=30 ms, *TR*=200 ms), (f, g, h, i, j) the same slices obtained by True-FISP pulse sequence (TE=30 ms, TR=500 ms).

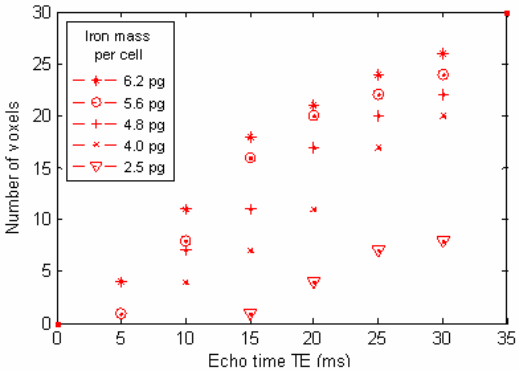

Fig. 2. Influence of TE on high-resolution 3D GE. Number of 40 μm^3 voxels with signal loss > 8 gray level with respect to background as a function of the TE and at different per-cell iron masses.

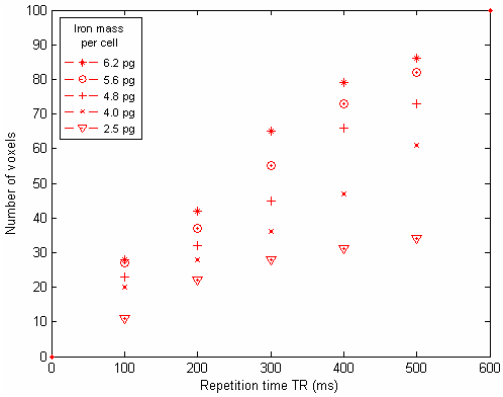

Fig. 3. Influence of TR on high-resolution 3D True-FISP. Number of 40×40×40 μm^3 voxels with signal loss > 8 gray level with respect to background as a function of the TR and at different per-cell iron masses.

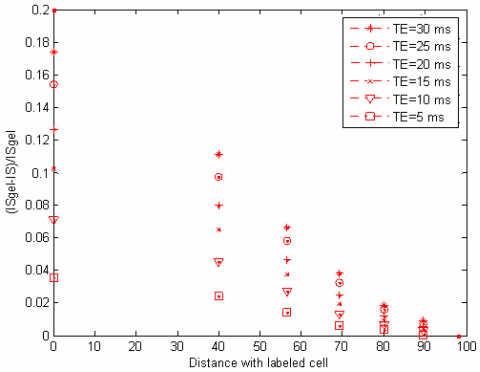

Fig. 4. Cell signal profile (high-resolution 3D GE 9.4T MRI). Relative signal loss as a function of the distance from the voxel containing the labeled cell at different TEs. The voxel size is 40×40×40 μm^3.

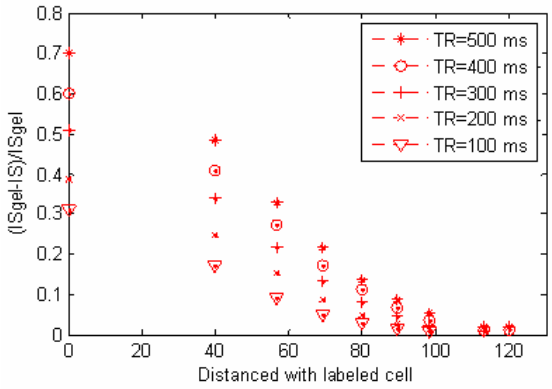

Fig. 5. Cell signal profile (high-resolution 3D True-FISP 9.4T MRI). Relative signal loss as a function of the distance from the voxel containing the labeled cell at different TRs. The voxel size is 40×40×40 μm^3.

Figure 2 shows the effect of TE in 3D GE pulse sequence on the detection sensitivity (similar to studies in [10]) for different iron masses. As this figure indicates, the image of the labeled cell spreads spatially with the increase of TE. The apparent MR volume of each labeled cell (in the output image) was determined by counting the number of voxels whose signal loss was higher than 8 gray levels (according to Weber ratio). These apparent volume values are also reported in Figure 3 as a function of the TR for True-FISP for different iron masses per cell. The apparent cell volume, in True-FISP was much larger than the actual size of a cell (the diameter of a cell is about 20 µm [13]) with respect to GE. The increase in the apparent volume with the TE in GE and TR in True-FISP was linear. However, a 2.5-fold increases in cellular iron load or the equivalent cell magnetization had only a moderate influence on the apparent size of the cell.

The spatial profiles of relative signal loss for GE and True-FISP are illustrated in Figures 4-5 as a function of the distance from the central voxel, for various TE and TR (cellular iron load=5.6 pg), respectively. Cell contrast spreads by up to 90 µm for GE and 120 µm for True-FISP from the central voxel and the intensity profile is broadened with increasing TE and TR in GE and True-FISP, respectively.

To examine the effect of resolution on the single cell detectability with GE and True-FISP, the voxel size of the output image was varied from 40 to 120 μm^3 for GE and 40 to 160 μm^3 for True-FISP. Figure 6 shows the relative signal loss in the central voxel (containing the cell) as a function of the voxel volume for different TEs for GE. Figure 7 shows the same function in different TRs for True-FISP. The signal loss falls noticeably with increasing voxel size at a 120 μm^3 resolution for GE and 160 μm^3 resolution for True-FISP. Thus, voxel sizes larger than 120 μm^3 for GE and 160μm^3 for True-FISP are unsuitable for single cell detection.

4. CONCLUSION

We presented a tool for evaluation and optimization of various MR pulse sequences and their parameters for molecular imaging without the need of costly measurements.

We investigated the detection of single cells labeled with iron oxide nanoparticles in a 9.4T MRI system. High resolution GE and True-FISP sequences detected individual labeled cells. The signal loss produced by the labeled cells enhanced and spread spatially with increasing echo times on GE sequences, and diminished

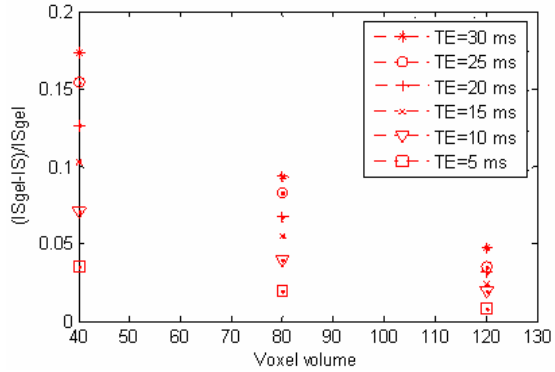

Fig. 6. Effect of resolution. Relative signal loss in the voxel containing the cell as a function of voxel size and for different TEs. The iron mass per cell is 5.6 pg. At the highest resolution (40 μm^3), the signal loss is maximum whatever the echo time.

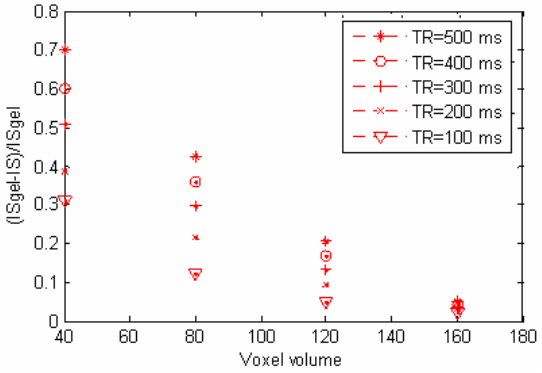

Fig. 7. Effect of resolution. Relative signal loss in the voxel containing the cell as a function of voxel size and for different TRs. The iron mass per cell is 5.6 pg. At the highest resolution (40 μm^3), the signal loss is maximum whatever the echo time.

rapidly with increasing voxel size. However, this effect can be obtained in True-FISP sequence by increasing the repetition time. According to our investigations, the True-FISP pulse sequence has higher sensitivity than GE. This simulation study provides the basis for experiments aimed at single cell detection with GE and True-FISP sequences *in vitro* and *in vivo.*

5. REFERENCES

[1] T. C. Yeh, W. Zhang, S. T. Ildstad and C. Ho, "In vivo dynamic MRI tracking of rat T-cells labeled with superparamagnetic iron-oxide particles," Magn Reson Med, vol. 33, pp. 200–208, 1995.

[2] B. J. Dardzinski, V. J. Schmithorst, S. K. Holland, G. P. Boivin, T. Imagawa, S. Watanabe, J. M. Lewis and R. Hirsch, "MR imaging of murine arthritis using ultrasmall superparamagnetic iron oxide particles," Magn Reson Imaging, vol. 19, pp. 1209–1216, 2001.

[3] A. Moore, E. Marecos, A. J. Bogdanov and R. Weissleder, "Tumoral distribution of long-circulating dextran-coated iron oxide nanoparticles in a rodent model," Radiology, vol. 214, pp. 568–574, 2000.

[4] V. Dousset, C. Delalande, L. Ballarino, B. Quesson, D. Seilhan, M. Coussemacq, E. Thiaudiere, B. Brochet, P. Canioni and J. M. Caille, "In vivo macrophage activity imaging in the central nervous system detected by magnetic resonance," Magn Reson Med, vol. 41, pp. 329–333, 1999.

[5] R. M. Lebel, R. S. Menon, and C. V. Bowen, "Relaxometry Model of Strong Dipolar Perturbers for Balanced-SSFP: Application to Quantification of SPIO Loaded Cells," Magn Reson Med, vol. 55, pp. 583–591, 2006.

[6] C. V. Bowen, X. Zhang, G. Saab, P. J. Gareau and B. K. Rutt, "Application of the static dephasing regime theory to superparamagnetic iron-oxide loaded cells," Magn Reson Med, vol. 48, pp. 52–61, 2002.

[7] P. Foster-Gareau, C. Heyn, A. Alejski and B. K. Rutt, "Imaging single mammalian cells with a 1.5 T clinical MRI scanner," Magn Reson Med, vol. 49, No. 5, pp. 968-971, 2003.

[8] C. Heyn, C. V. Bowen, B. K. Rutt and P. J. Foster, "Detection threshold of single SPIO-labeled cells with FIESTA," Magn Reson Med, vol. 53, pp. 312-320, 2005.

[9] E. M. Shapiro, K. Sharer, S. Skrtic and A. P. Koretsky, "In vivo detection of single cells by MRI," Magn Reson Med, vol. 55, No. 2, pp. 242-2354, 2006.

[10] P. smirnov, F. Gazeau, J. C.Beloei1, B. T. Doan, C. Wilhelm and B. Gillet, "Single cell detection by gradient echo 9.4 T MRI: a parametric study," Contrast Med. Mol. imaging, vol. 1, pp. 165-174, 2006.

[11] C. Faber, C. Heil, B. Zahneisen, D. Z. Balla and R. Bowtell, "Sensitivity to local dipole fields in the CRAZED experiment: An approach to bright spot MRI," J Magn Reson, pp. 1-10, 2006.

[12] J. F. Schenck, "The role of magnetic susceptibility in magnetic resonance imaging: MRI magnetic compatibility of the first and second kinds," Med Phys, vol. 23, pp. 815–843, 1996.

[13] C. E. Sjogren, C. Johansson, A. Naevestad, P. C. Sontum, K. Briley-Saebo and A. K. Fahlvik, "Crystal size and properties of superparamagnetic iron oxide (SPIO) particles," Magn Reson Imaging, vol. 15, pp. 55–67, 1997.

[14] Y. X. J. Wang, S. M. Hussain and G. P. Krestin, "Superparamagnetic iron oxide contrast agents: physicochemical characteristics and applications in MR imaging," Eur. Radiol, vol. 11, pp. 2319–2331, 2001.

[15] H. Benoit-Cattin, G. Collewet, B. Belaroussi, H. Saint-Jalmes and C. Odet, "The SIMRI project: a versatile and interactive MRI simulator," J Magn Reson, vol. 173, Issue 1, pp. 97-115, 2005.

[16] R. C. Gonzalez and R. E. Woods, "Digital Image Processing," 2nd Edition, Prentice Hall, 2002.